Multi-MHz time-of-flight electronic bandstructure imaging of graphene on Ir(111)

C. Tusche' , P. Goslawski, D. Kutnyakhov, M. Ellguth, K. Medjanik, H. J. Elmers, S. Chernov, R. Wallauer, D. Engel, A. Jankowiak, and G. Schönhense

Citation: Appl. Phys. Lett. **108**, 261602 (2016); doi: 10.1063/1.4955015
View online: http://dx.doi.org/10.1063/1.4955015
View Table of Contents: http://aip.scitation.org/toc/apl/108/26
Published by the American Institute of Physics

Multi-MHz time-of-flight electronic bandstructure imaging of graphene on Ir(111)

C. Tusche,[1,2,a)] P. Goslawski,[3] D. Kutnyakhov,[4] M. Ellguth,[1,4] K. Medjanik,[4,5] H. J. Elmers,[4] S. Chernov,[4] R. Wallauer,[4] D. Engel,[3] A. Jankowiak,[3] and G. Schönhense[4]
[1]*Max-Planck-Institut für Mikrostrukturphysik, Weinberg 2, 06120 Halle, Germany*
[2]*Peter Grünberg Institut (PGI-6), Forschungszentrum Jülich GmbH, 52425 Jülich, Germany*
[3]*Helmholtz-Zentrum Berlin für Materialien und Energie GmbH, 12489 Berlin, Germany*
[4]*Institut für Physik, Johannes Gutenberg-Universität, 55128 Mainz, Germany*
[5]*MAX IV Laboratory, Ole Römers vag 1, 22363 Lund, Sweden*

(Received 2 March 2016; accepted 13 May 2016; published online 27 June 2016)

In the quest for detailed spectroscopic insight into the electronic structure at solid surfaces in a large momentum range, we have developed an advanced experimental approach. It combines the 3D detection scheme of a time-of-flight momentum microscope with an optimized filling pattern of the BESSY II storage ring. Here, comprehensive data sets covering the full surface Brillouin zone have been used to study faint substrate-film hybridization effects in the electronic structure of graphene on Ir(111), revealed by a pronounced linear dichroism in angular distribution. The method paves the way to 3D electronic bandmapping with unprecedented data recording efficiency. *Published by AIP Publishing.* [http://dx.doi.org/10.1063/1.4955015]

Photoelectron spectroscopy is recognized to be a very powerful approach to study the electronic structures of many materials under hot debate today. In particular, the discovery of material classes with non-trivial topology of their electronic states[1] and related materials, like graphene,[2] with massless "Dirac" fermions created a strong driving force for the improvement of experimental means to access their electronic structures, in particular, by angle resolved photoemission spectroscopy (ARPES).

For systems such as topological insulators (TI), where a locking of the electron spin to the crystal momentum is decisive for the robustness and protection of these states, conventional ARPES becomes a time-consuming task. A fundamental improvement to this situation was recently introduced as momentum microscopy with the optional combination with two-dimensional (2D) spin filtering.[3] A momentum microscope uses the imaging properties of a cathode lens to form a 2D image of the photoemission intensities directly in reciprocal space. As these images typically cover the full surface Brillouin zone (SBZ) of the sample, mechanical scanning with its undesirable variation of the direction of the electric field vector is avoided. The rapid measurement of 2D cuts through the band structure provides comprehensive information on the near-surface electronic structure.[4,5]

In many cases, one is interested in the complete three-dimensional (3D) dispersion of bands represented as the data matrix (k_x, k_y, and E_B), where k_x and k_y are the in-plane crystal momenta, and E_B is the binding energy. By combining the momentum microscope with a time-of-flight (ToF) energy analyzer, these 3D data sets can be measured simultaneously. Such comprehensive data sets of the electronic structure of the Mo(110) surface recently revealed the presence of an anomalous "Dirac" cone like state[6] previously only known for the W(110)[7] surface which has a much larger spin-orbit coupling.

Figure 1(a) shows the working principle of a conventional ToF energy analyzer. Electrons excited by a pulsed photon source travel along the spectrometer tube at low kinetic energies. In the simplest case, these drift energies correspond closely to the kinetic energy of the electron. A space- and time-resolving detector then registers each electron by its arrival coordinate (x, y, τ), being converted to the momentum and energy scale. To avoid fast electrons from the next photon pulse overtaking slow electrons from the previous ones, only one electron packet travels through the spectrometer until the slowest electrons have arrived at the detector. This generally results in a rather low repetition rate in the range of 1 MHz.

The low repetition rate, however, poses a fundamental limitation to the measurement efficiency of the ToF analyzer, diminishing the advantage of parallel acquisition. The reason is that Coulomb repulsion within the electron ensemble sets a principal limit for the maximum number of electrons that can be emitted per pulse. While the interaction of an electron with the average charge distribution of all other electrons (space-charge interaction) is a deterministic process that can be partly corrected in a momentum microscope,[8] individual e-e processes lead to an irreversible broadening of the ensemble. These space-charge effects may be avoided by increasing the repetition rate, rather than the intensity of a single pulse.

Figure 1(b) shows the working principle of the ToF momentum microscope for the case of a photoelectron energy of 16 eV. The electron optical design follows the same principle as the instrument with dispersive energy filter as outlined in Ref. 3. The first k-image is formed in the Fourier plane of the electrostatic cathode lens. Then several lens elements create a first and second real image, the latter at the entrance to the drift tube. An advantage of the long field-free drift section is the fact that most of the electron path is traveled at constant velocity, enabling a direct conversion from ToF to the energy scale. Additionally, the image curvature at

[a)]Electronic mail: c.tusche@fz-juelich.de

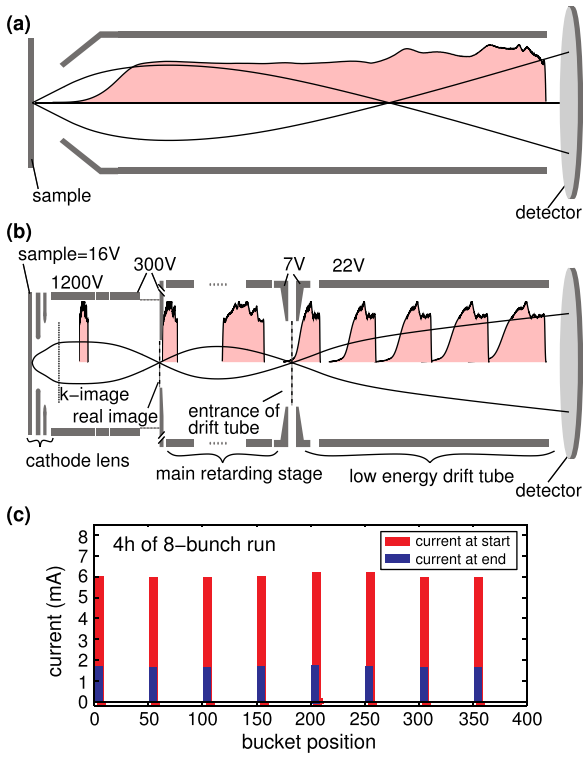

FIG. 1. (a) Working principle of a ToF spectrometer. Photoelectrons (black lines) from the sample are focused on the (x, y, τ)-resolving detector. The underlaid spectrum indicates the emitted electron distribution dispersed in time. (b) Layout of the ToF momentum microscope. The k-image is formed by the cathode lens and projected onto the detector. Emission spectra from several bunches travel through the field free drift tube at the same time. (c) Fill pattern and current distribution at the beginning and end of the 4 h long 8-bunch run.

the detector is weak and hence the radial dependence of the ToF is negligible. When the electrostatic potential at the intermediate image (7 V in Fig. 1(b)) is chosen lower than the drift tube potential (22 V in Fig. 1(b)), the high intensity tail of secondary electrons is blocked, and the slowest electrons inside the drift tube maintain a finite ToF.

The interplay between the desired energy resolution (by low drift energy) and the width of the energy distribution defines the time interval needed for energy dispersion, and hence the period of the photon pulses. The ToF difference between the high-energy leading edge of the distribution, corresponding to the Fermi energy (E_F), and the low-energy cutoff (here E_F–7 eV) should not exceed the photon-pulse period (here: 100 ns). For standard work, 100–300 ns periods are ideal, corresponding to 3–10 MHz repetition rate. In the present experiment, the total count rate was about 5 Mcps, i.e., less than one detected electron per photon pulse. We estimate that the total electron yield (including secondary electrons) is 1–2 orders of magnitude larger. At maximum, 10^2 electrons are ejected within 50 ps and from a 80 μm diameter disk on the sample. Under these conditions, the space-charge effect is negligible. The efficiency of the measurement increases linearly with the photon pulse repetition rate until the time-resolution of the detector limits the desired energy resolution.

The photon pulse structure generated by the synchrotron is defined by the electron fill pattern, which in principle can be chosen at will restricted by certain conditions. One constraint is the number of places or buckets h, in which electrons can be stored, determined by the ratio of revolution frequency f_0 and radio frequency $f_{rf} = h \cdot f_0$, restoring the energy electrons lost by radiating. Many storage rings (such as BESSY II) are operated at 500 MHz, others (e.g., MAX II and IV) run at 100 MHz. The standard operating conditions of storage rings put main emphasis on maximum photon flux. For time-resolved experiments, single- or few-bunch modes are offered, usually for few weeks per year only.

For instance, BESSY II offers a multibunch filling of 300 buckets each with ≈0.9 mA for nearly 90% of the user time, including a 200 ns long gap. For conventional ToF experiments, one high current bunch with 4 mA is stored in the middle of the gap producing a 1.25 MHz photon signal. In order to provide a pure single bunch signal when running in this multibunch "hybrid" mode, the accelerator community is working on separation schemes such as the "pulse picking resonant excitation"[9] and the MHz-chopper.[10] Three weeks per year a true single bunch mode is provided by injecting electrons up to 12 mA in one bucket only. In all cases, the time structure is restricted to a repetition rate of 1.25 MHz, far from optimum for ToF-based band-mapping.

The experiment described here was the first asking for a "few bunch" mode at BESSY II aiming for a higher repetition rate of about 10 MHz. Due to the very flexible "fill pattern generator software" controlling the complete injection procedure, it was possible to set up this fill pattern in a dedicated machine commissioning shift. Eight buckets with an equidistant spacing of 100 ns in the 800 ns long fill have been populated with 6 mA each and used in decay mode for nearly 4 h (see Fig. 1(c)). Topping up the current was not yet implemented for this mode.

The special filling pattern results in an 8 times increased counting rate of photoelectrons detected by the momentum microscope, over single bunch operation. Together with the measurement of all possible emission directions, this is of particular advantage when studying faint anomalies in the electronic structure. A paradigmatic case is the hybridization of states across the interface between Ir(111) and a monolayer of graphene. The π-band of graphene shows a pronounced linear dispersion reflecting the zero effective mass of Dirac fermions, being the origin of an ultra-high group velocity and a large spin relaxation length.[11,12] This Dirac-cone state is, unlike such states in many TIs, not located at the center of the SBZ, but at the $\overline{K}$ points at the SBZ's corners.

Figure 2 shows selected sections through the measured $I(k_x, k_y, E_B)$ spectral function of monolayer graphene on Ir(111) for an energy range between E_F and E_F–3.5 eV. With a fixed setting of the momentum microscope high $k_{||}$-resolution is obtained in an energy interval of about 10% of the transferred spectrum. With the given cut-off energy of 7 eV (see Fig. 1(b)), this results in a usable energy range of 0.7 eV, before chromatic aberration degrades the $k_{||}$ resolution. To acquire a larger energy range, the energy axis was shifted in steps of 0.5 eV by adjusting only the sample potential. We combine 7 individual exposures of 5 min each to cover a total of 3.5 eV in a data set of 482 energy slices (≈7.7 meV per slice). Having acquired the complete valence bandstructure within 35 min, the data are analyzed in detail offline.

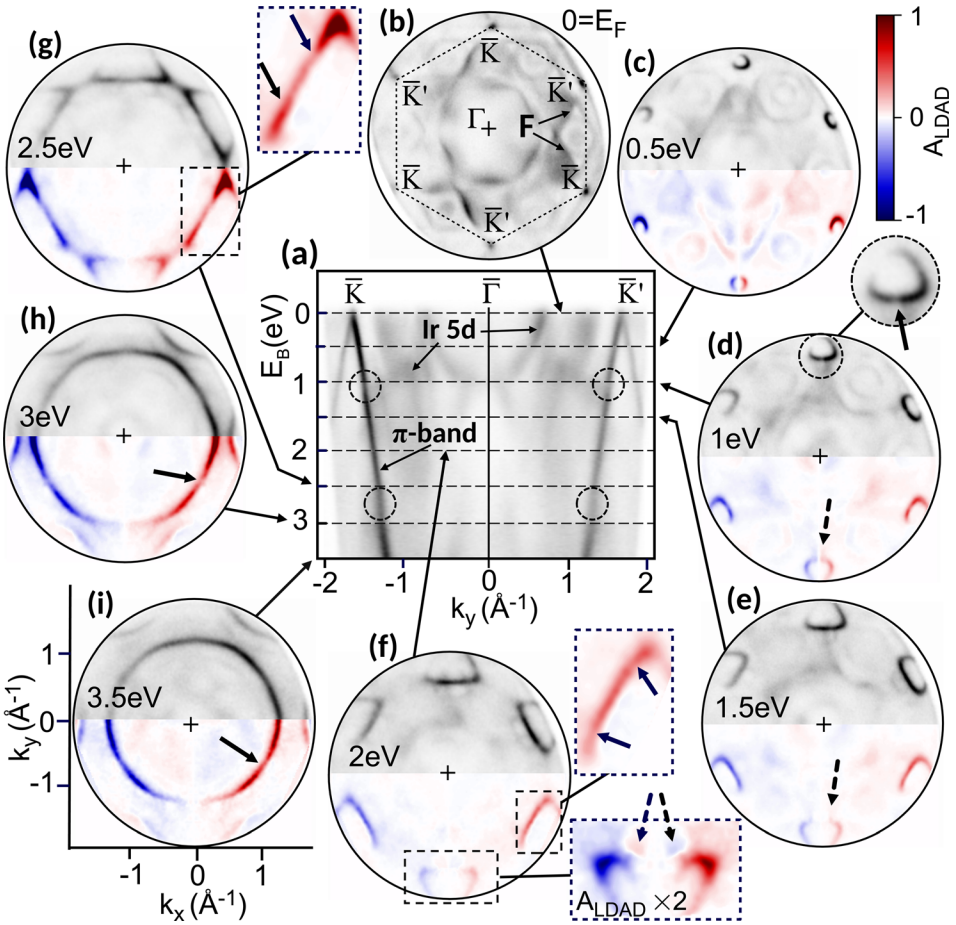

FIG. 2. Sections through the spectral function of graphene on Ir(111) measured at $h\nu = 22$ eV. (a) $\overline{K} - \overline{\Gamma} - \overline{K'}$ direction showing the linear energy dispersion of the π-band and the Dirac crossing close to E_F. The full 3D data matrix consists of 482 E = const. momentum discs, 8 of which are shown in ((b)–(i)) on a linear gray scale (upper half) and as LDAD plot (lower half). Dashed circles and arrows mark hybridization regions, and "F" (in (b)) the contour of the Ir Fermi surface.

Since the momentum microscope measures the full 3D matrix $I(k_x, k_y, E_B)$, 2D sections can be projected in any desired plane. For instance, the band dispersion along $\overline{K}$–$\overline{\Gamma}$–$\overline{K'}$ is shown in Fig. 2(a). The prominent feature is the π-band of graphene with its linear dispersion and Dirac point close to E_F. The Ir 5d bands are visible as weaker features. The interaction of the graphene π-system with the substrate leads to gaps and kinks in the dispersion of the π-band. We recognize the well-known hybridization gaps[13] due to avoided crossings of the graphene π-band with Ir 5d bands at $E_B \approx 1.2$ and 2.7 eV, marked by dashed circles.

For a comprehensive analysis, it is favorable to look at the constant-energy sections (corresponding to constant ToF), 8 of which are shown in Figs. 2(b)–2(i). We refer to these sections as "momentum discs." They are characterized by a linear (k_x, k_y)-scale which stays constant, independent of energy. Details on momentum microscopy are found in recent reviews.[14,15] Here, the momentum discs have a diameter of about 3.7 Å^{-1}, slightly larger than the SBZ. Their outer border is close to the photoemission horizon, corresponding to an emission angle of 90°. In other words, the data shown represent the full half-space of emission directions above the sample surface.

The disc at E_F (Fig. 2(b)) shows the six tips of the Dirac cones at the $\overline{K}$ points. The characteristic sixfold feature marked "F" is the contour of the Ir Fermi surface. With increasing binding energy, the Dirac cones widen with almost circular cross section (c) and then become triangular ((d)–(f)).[11] At $E_B = 2.5$ eV (g), the corners of the triangles touch each other forming a hexagon, developing into a circular contour ((h) and (i)). The upper hybridization region that looks rather diffuse in the E-k section (a) shows up as a very narrow gap in the triangular cross section of the Dirac cone; see enlarged detail of (d).

Intensity differences between the left and right side of the momentum discs reflect the linear dichroism in the photoelectron angular distribution (LDAD),[6] with the p-polarized photon beam incident in the k_x-k_z plane. Since the momentum microscope detects all emission directions simultaneously in a fixed geometry, quantitative LDAD asymmetries (A_{LDAD}) are directly calculated for each momentum disc, considering the symmetry of the surface. The LDAD exists already in the non-relativistic limit and has its origin in a non-coplanar arrangement of the electric field vector, the quantization axis of the initial-state wavefunction and the photoelectron momentum. Owing to its pure p_z-character, the π-band is expected to show a huge A_{LDAD}. For the π-band in graphite, at $h\nu = 22$ eV, a circular dichroism of up to 50% has been found,[16] in quantitative accordance with our result for graphene.

Hybridization of the graphene π-band with Ir 5d-bands leads to a mixing of p_z and d partial waves. Since the LDAD is sensitive to the partial-wave composition of the initial state, this mixing shows up in the dichroism signal. The large LDAD originating from the p_z-symmetry is reflected by a local enhancement of the dichroism in the Ir bands, denoted by dashed arrows in Figs. 2(d)–2(f). Likewise, the admixture of Ir d-character to the π-wavefunction causes a reduction of the LDAD in Figs. 2(g)–2(i) (marked by solid arrows). Moreover, the π-band appears more diffuse and shows

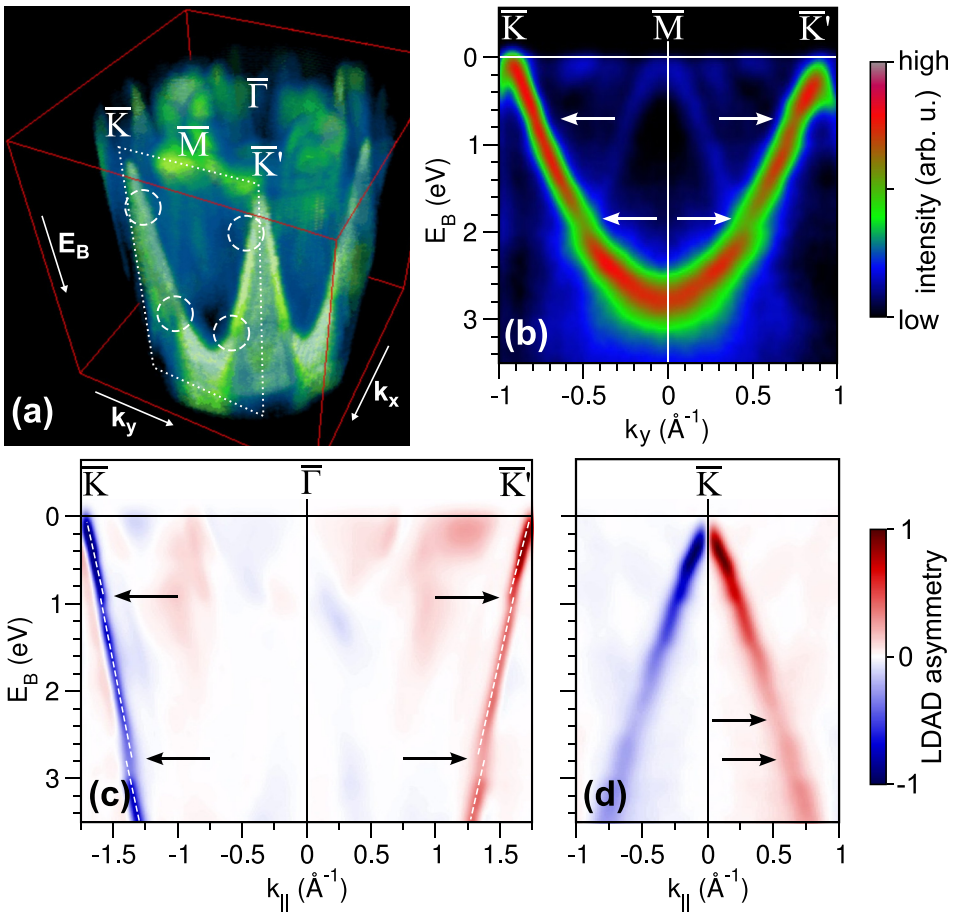

FIG. 3. (a) 3D view of the spectral function $I(k_x, k_y, E_B)$ of monolayer graphene on Ir(111). (b) "Non-canonical" section along $\overline{K} - \overline{M} - \overline{K'}$, marked by the dotted rectangle in (a). (c) LDAD asymmetry along the $\overline{K} - \overline{\Gamma} - \overline{K'}$ direction, and (d) across the Dirac cone. Circles and arrows mark hybridization regions, dashed lines in (c) serve as a guide to the eye.

characteristic kinks in hybridization regions,[12] also visible in the constant energy contours in the insets of Figs. 2(f) and 2(g).

A perspective view showing the 3D topology of the π-band is given in Fig. 3(a). We note that this view shows the as-measured raw data of the combined 7 exposures. A particularly interesting k-space location is shown in Fig. 3(b). This is a "non-canonical" E-k section along $\overline{K}$–$\overline{M}$–$\overline{K'}$ that does not cross the $\overline{\Gamma}$ point. The false color scale emphasizes the weak substrate states, revealing two hybridization gaps due to avoided crossings of the π-band with Ir 5d bands at $E_B \approx 0.7$ and 1.8 eV. The LDAD shown in Figs. 3(c) and 3(d) reveals that the pronounced kinks in the intense π-band are directly connected with a reduction of the LDAD asymmetry due to the contribution of the Ir-states.

In summary, the high average count rate of about 5×10^6 per second provided by the 8-bunch mode allows a rapid mapping of the spectral function in the full SBZ. For graphene on Ir(111), a multitude of hybridization points between the π-band of graphene and the Ir 5d-bands was analyzed. A special emphasis was put on the LDAD that is directly accessible due to the simultaneous detection of all emission directions. We see in the hybridization region an enhancement of the LDAD in the Ir bands due to admixture of p_z-, and a reduction in the graphene π-band due to admixture of d-contributions. The linear dichroism signal turned out to be a sensitive probe of these subtle effects in the band structure.

The present experiment has triggered a discussion about establishing a "few bunch" operation mode optimizing the time structure for most efficient use in the BESSY II community, which is still ongoing. Besides the ToF momentum microscope, another user group[17] also profits from the 8-bunch fill, gaining a factor of 4 in intensity and improving their signal to noise ratio by a factor of 2.

In the future, separation concepts for simultaneously providing optimized time structures of the photon source suggest a most efficient use of ToF momentum microscopy at modern synchrotron sources. For instance, operating the storage ring close to a resonance and using non-linear effects provides a second orbit resulting in a multi-beam machine.[18] By exciting individual bunches, the second orbit can be populated at will. Currently, the proof of principle experiments are conducted at BESSY II, and might pave the way to offer a "few bunch" mode simultaneously to a multibunch fill.

Sincere thanks go to A. Oelsner (Surface Concept GmbH) for valuable technical support, to K. Horn (Fritz-Haber-Institute) for helpful comments and critical reading of the manuscript, and to J. Kirschner (MPI-Halle) for his continuous support and encouragement. Funding by BMBF (05K12EF1, 05K12UM2 and 05K13UM1) is gratefully acknowledged.

[1]M. Z. Hasan and C. L. Kane, Rev. Mod. Phys. **82**, 3045 (2010).
[2]A. H. Castro Neto, F. Guinea, N. M. R. Peres, K. S. Novoselov, and A. K. Geim, Rev. Mod. Phys. **81**, 109–162 (2009).
[3]C. Tusche, A. Krasyuk, and J. Kirschner, Ultramicroscopy **159**, 520 (2015).
[4]S. Roy, H. L. Meyerheim, A. Ernst, K. Mohseni, C. Tusche, M. G. Vergniory, T. V. Menshchikova, M. M. Otrokov, A. G. Ryabishchenkova, Z. S. Aliev *et al.*, Phys. Rev. Lett. **113**, 116802 (2014).

[5]S. Suga, C. Tusche, Y.-I. Matsushita, M. Ellguth, A. Irizawa, and J. Kirschner, New J. Phys. **17**, 083010 (2015).
[6]S. V. Chernov, K. Medjanik, C. Tusche, D. Kutnyakhov, S. A. Nepijko, A. Oelsner, J. Braun, J. Minár, S. Borek, H. Ebert *et al.*, Ultramicroscopy **159**, 453 (2015).
[7]K. Miyamoto, A. Kimura, K. Kuroda, T. Okuda, K. Shimada, H. Namatame, M. Taniguchi, and M. Donath, Phys. Rev. Lett. **108**, 066808 (2012).
[8]G. Schönhense, K. Medjanik, C. Tusche, M. de Loos, B. van der Geer, M. Scholz, F. Hieke, N. Gerken, J. Kirschner, and W. Wurth, Ultramicroscopy **159**, 488 (2015).
[9]K. Holldack, R. Ovsyannikov, P. Kuske, R. Müller, A. Schälicke, M. Scheer, M. Gorgoi, D. Kühn, T. Leitner, S. Svensson *et al.*, Nat. Commun. **5**, 4010 (2014).
[10]D. F. Förster, B. Lindenau, M. Leyendecker, F. Janssen, C. Winkler, F. O. Schumann, J. Kirschner, K. Holldack, and A. Föhlisch, Opt. Lett. **40**, 2265 (2015).
[11]E. Rotenberg and A. Bostwick, Synth. Met. **210**, 85 (2015).
[12]M. Kralj, I. Pletikosić, M. Petrović, P. Pervan, M. Milun, A. T. N'Diaye, C. Busse, T. Michely, J. Fujii, and I. Vobornik, Phys. Rev. B **84**, 075427 (2011).
[13]I. Pletikosić, M. Kralj, P. Pervan, R. Brako, J. Coraux, A. T. N'Diaye, C. Busse, and T. Michely, Phys. Rev. Lett. **102**, 056808 (2009).
[14]S. Suga and C. Tusche, J. Electron Spectrosc. Relat. Phenom. **200**, 119 (2015).
[15]G. Schönhense, K. Medjanik, and H.-J. Elmers, J. Electron Spectrosc. Relat. Phenom. **200**, 94 (2015).
[16]G. Schönhense, C. Westphal, J. Bansmann, and M. Getzlaff, Europhys. Lett. **17**, 727 (1992).
[17]R. Doerner, "Coltrims experiments, Johann Wolfgang Goethe-Universität," private communication (2015).
[18]P. Goslawski, J. Feikes, K. Holldack, A. Jankowiak, R. Ovszannikov, M. Ries, M. Ruprecht, A. Schälicke, and G. Wüstefeld, in *Proceedings of IPAC2016*, Busan, Korea (2016), p. THPMR017.